International Journal of Pharmaceutics 624 (2022) 121959

Contents lists available at ScienceDirect

International Journal of Pharmaceutics

journal homepage: www.elsevier.com/locate/ijpharm

Folic acid-mesoporous silicon nanoparticles enhance the anticancer activity of the p73-activating small molecule LEM2

Ana Sara Gomes [a,b,c], Alexandra Correia [b], Antti Rahikkala [b], Ermei Mäkilä [d], Madalena M. Pinto [c,e], Emília Sousa [c,e], Jarno Salonen [d], Lucília Saraiva [a], Hélder A. Santos [b,f,*]

[a] LAQV/REQUIMTE, Laboratório de Microbiologia, Departamento de Ciências Biológicas, Faculdade de Farmácia, Universidade do Porto, 4050-31b Porto, Portugal
[b] Drug Research Program, Division of Pharmaceutical Chemistry and Technology, Faculty of Pharmacy, University of Helsinki, Helsinki FI-00014, Finland
[c] Laboratory of Organic and Pharmaceutical Chemistry (LQOF), Department of Chemical Sciences, Faculty of Pharmacy, University of Porto, Rua de Jorge Viterbo Ferreira, 228, 4050-313 Porto, Portugal
[d] Laboratory of Industrial Physics, Department of Physics, University of Turku, FI-20014 Turku, Finland
[e] Interdisciplinary Centre of Marine and Environmental Research (CIIMAR), Terminal de Cruzeiros do Porto de Leixões, Av. General Norton de Matos s/n, 4450-208 Matosinhos, Portugal
[f] Department of Biomedical Engineering and W.J. Kolff Institute for Biomedical Engineering and Materials Science, University Medical Center Groningen / University of Groningen, 9713 AV Groningen, the Netherlands

ARTICLE INFO

Keywords:
Porous silicon
Nanoparticle
P73
Anticancer
Small molecule
Bioavailability

ABSTRACT

Many drugs with anticancer potential fail in their translation to the clinics due to problems related to pharmacokinetics. LEM2 is a new dual inhibitor of MDM2/mutp53-TAp73 interactions with interesting *in vitro* anticancer activity, which opens new hopes as an unconventional anticancer therapeutic strategy against cancers lacking p53 or with impaired p53 pathways. As others xanthone derivatives, LEM2 has limited aqueous solubility, posing problems to pursue *in vivo* assays, and therefore limiting its potential clinical translation. In this work, a mesoporous silicon (PSi)-based nanodelivery system was developed with folate functionalization (APTES-TCPSi-PEG-FA) for targeted delivery, which successfully increased LEM2 solubility when compared to bulk LEM2, evidenced in payload release study. Such effect was reflected on the increase of LEM2 cytotoxicity in HCT116 and MDA-MB-231 cancer cells when treated with LEM2-loaded APTES-TCPSi-PEG-FA, by reducing cell viability lower than 50% in comparison with bulk LEM2. Despite the reduced LEM2 loading degree, which still limits its application in further *in vivo* assays, the results obtained herein recognize PSi-based nanodelivery systems as a promising strategy to improve LEM2 anticancer activity and bioavailability, which will be relevant for the potential use of this potent TAp73 activator in anticancer therapy.

1. Introduction

Despite the advances in drug discovery and development, many small molecules fail during this process due to physicochemical properties, pharmacokinetic and/or toxicity-related problems, among others (Waring et al., 2015). In this context, nanotechnology can offer the opportunity to overcome drug-related limitations (Mirza, 2014), such as masking the physicochemical properties of small molecules, increasing efficacy and safety by tissue- or cell-targeted therapies, protecting from degradation or clearance and controlling drug release (Patra et al., 2018). Considering the physicochemical property solubility, compounds with low solubility and high permeability (class II, Biopharmaceutic Classification System (BCS)), or with low solubility and low permeability (class IV, BCS) are eligible to nanodelivery system design (Amidon et al., 1995; Lipinski, 2002; Williams et al., 2013).

There is a myriad of nanomaterials from different sources to produce nanocarriers for drug delivery, *i.e.,* lipidic (*e.g.*, micelles, liposomes, solid-lipid NPs), polymeric (*e.g.*, dendrimers, polymer-drug conjugates,

Abbreviations: APTES, 3-aminopropyltriethoxysilane; DLS, dynamic light scattering; EE (%), entrapment efficiency in percentage; FA, folic acid; FR, folate receptor; LD(%), loading degree in percentage; NP, nanoparticle; PdI, polydispersity index; PEG, polyethylene glycol; RT, room temperature; TCPSi, thermally carbonized porous silicon.

* Corresponding author at: Department of Biomedical Engineering and W.J. Kolff Institute for Biomedical Engineering and Materials Science, University Medical Center Groningen / University of Groningen, 9713 AV Groningen, the Netherlands.
E-mail address: h.a.santos@umcg.nl (H.A. Santos).

https://doi.org/10.1016/j.ijpharm.2022.121959
Received 5 March 2022; Received in revised form 18 June 2022; Accepted 21 June 2022
Available online 2 July 2022

nanospheres), cell membrane-derived (*e.g.* cancer cells, red blood cells, macrophages), and inorganic (*e.g.*, gold, mesoporous silicon, carbon nanotubes) (Din et al., 2017). The selection of the most suitable nanomaterial is based on the bio-physicochemical features of the drug (Patra et al., 2018). The efficacy of these nanodelivery systems depends on their size, shape, target selectivity, efficiency of uptake, drug concentration and release kinetics, as well as on biological barriers and physicochemical properties of the host environment (Misra et al., 2010).

Mesoporous stands for materials with pore diameter ranging from 2 to 50 nm (Sing et al., 1985), and are designed to allow high payloads of drugs and protect them from premature release and degradation before reaching the target site (Prestidge et al., 2007). Uppon loading it has been reported that the drug suffers a transition to an amorphous state, due to physical adsorption and physical confinement within the pore (Makila et al., 2014). The amorphous form is associated with higher internal energy with enhanced thermodynamic and kinetic properties (solubility and dissolution rate) in opposition to the bulk drug that presents a crystalline form (Hancock and Parks, 2000).

Mesoporous silicon (PSi)-based materials are attractive due to their unique physicochemical properties and potential versatile biomedical applications, specifically in cancer therapy and bioimaging (Shahbazi et al., 2012). PSi nanoparticles (NPs), have been shown as drug delivery vectors for a wide variety of chemotherapeutic agents, such as cisplatin, doxorubicin, and sorafenib, which are drugs with anticancer activity but suffering from poor cellular selectivity or undesirable side effects (Anglin et al., 2008; Li et al., 2018). Likewise, PSi has proven to be biodegradable, being dissolved into orthosilicic acid species, which are known to be harmless to cells and easily excreted in urine (Hon et al., 2012; Li et al., 2018). PSi NPs are characterized by high surface-to-volume ratio, large specific surface area and pore volume, and a robust framework with chemical, thermal, and mechanical stability (Salonen and Lehto, 2008). The possibility to tune the pore size and surface chemistry allows the PSi NPs to act as a selective storage while taking into acount the size and hydrophobicity of drugs (Salonen et al., 2008). Freshly produced PSi is reactive due to its surface hydride groups being necessary further stabilization, as the case of thermally carbonized (TC)PSi suitable for the loading of hydrophobic drugs (Santos et al., 2014). In the present work, to further facilitate surface functionalization reactions, TCPSi was treated with 3-aminopropyltriethoxysilane (APTES) that confers an $–NH_2$-terminated surface (Makila et al., 2012). Therefore, PSi surface is amenable to be functionalized with different biomolecules for targeted delivery of the cargo (Rosenholm et al., 2012). For the interest of the present work, one promising strategy for cancer cell targeting is the decoration of NPs with folic acid (FA), the natural ligand of folate receptor (FR) that mediates NPs internalization. FR is often overexpressed in cancer cells (when comparing to normal non-proliferating cells) due to their intense proliferation, which contributes to selectivity (Xia and Low, 2010).

The transcriptional factor p73 belongs to the p53 protein family. There are several p73 isoforms with different biological meanings, being that the N-terminal transactivation domain (TA)p73 isoform guarantees cellular homeostasis and tumor suppression (Candi et al., 2014). Although TAp73 is rarely mutated, its activity could be halted by overexpression of negative regulators, particularly the murine double minute 2 and 4 (MDM2/4) proteins, or by heterodimerization with mutant p53, contributing for tumorigenesis (Ramos et al., 2020). Therefore, TAp73 has been studied as an interesting target for cancer treatment, particularly in mutant p53 or p53-null contexts, and different strategies of drug development have been pursued regarding TAp73 activation (Gomes et al., 2021; Ramos et al., 2020). Particularly, the small molecule LEM2, 1-carbaldehyde-3,4-dimethoxy-9*H*-xanthen-9-one, which operates by disrupting protein–protein interactions between tumor suppressive TAp73 isoform and mutant p53 or MDM2, is a xanthone derivative with TAp73-dependent anticancer activity against a wide panel of cancer cell lines, including colorectal carcinoma, breast adenocarcinoma, and patient-derived neuroblastoma cells, without inducing genotoxicity (Gomes et al., 2019; Malta et al., 2021). However, LEM2 has demonstrated low solubility in aqueous solutions, with values lower than 0.1 mg/mL, being considered practically insoluble according to European Pharmacopoeia solubility criteria (Council of Europe, 2022). This has limited the study of LEM2 *in vivo*, counteracting its further development as an anticancer drug candidate.

Therefore, in order to improve LEM2 bioavailability, different approaches were endorsed, such as the development of nanostructured lipid carriers envisioning topical administration for melanoma treatment (Malta et al., 2021). The present study focus on the development of an alternative nanodelivery system for LEM2 based on PSi NPs functionalized with FA, envisioning oral or intravenous administration routes for solid tumors treatment, such as colorectal carcinoma and breast adenocarcinoma.

2. Material and methods

2.1. General

All chemicals and solvents used were purchased from Sigma-Aldrich (Espoo, Finland). Purified water was obtained by Milli-Q® Integral 15 Water Purification System (Merck Millipore, Burlington, Massachusetts, USA). NPs were dispersed with ultrasound either with bath sonication or tip sonication (30% amplitude, 10 s), using a stepped microtip (no. 630-0423, Sonics & Materials Inc., Newtown, Connecticut, USA) powered by a VCX 750 ultrasonic processor (Sonics & Materials Inc.). Centrifugations were performed in L-70 Ultracentrifuge (Beckman, Brea, California, USA) or 5415D Centrifuge (Eppendorf AG, Germany, Hamburg). RPMI-1640 medium, L-glutamine, non-essential amino acids (NEAA), penicillin (100 IU/mL), streptomycin (100 mg/mL) and trypsin (2.5%) were purchased from HyClone™ (GE Healthcare Life Sciences, Little Chalfont, Buckinghamshire, UK). Heat inactivated fetal bovine serum (FBS), Hank's balanced salt solution (HBSS) 10× and Versene were from Gibco® (ThermoFisher Scientific, Waltham, Massachusetts, USA). Triton X-100 was purchased from Merck Millipore. 1-Carbaldehyde-3,4-dimethoxy-9*H*-xanthen-9-one (LEM2) was synthesized and purified as described in (Gomes et al., 2019).

2.2. Production of APTES-TCPSi NPs

The core of 3-aminopropyltriethoxysilane modified thermally carbonized mesoporous silicon (APTES-TCPSi) NPs was produced as described in (Makila et al., 2012). Briefly, the PSi structure was obtained by electrochemical anodization of monocrystalline, boron-doped p^+-type Si(1 0 0) wafers with a resistivity of 0.01–0.02 Ωcm with a 1:1 (v/v) hydrofluoric acid (38%)-ethanol electrolyte. A multilayer structure consisting of alternating low and high porosity layers was formed, where the high porosity layers function as fracture planes. The multilayer was finally released as a freestanding film using an electropolishing current. The multilayer PSi free-standing films were then stabilized by thermal carbonization (TCPSi) using a two-stage treatment at 500 and 820 °C, as described in (Makila et al., 2012). To obtain APTES-TCPSi, the multilayer TCPSi films were pre-treated with 1:1 (v/v) aqueous hydrofluoric acid (HF) (38%)-ethanol solution to partially reactivate the stabilized surface by producing hydroxyl groups for silanization. The HF-treated TCPSi films were immersed into a 10 vol-% APTES-anhydrous toluene solution for 1 h at 25 °C. After the reaction, the excess silane was removed by washing with copious amounts of anhydrous toluene and ethanol. The silane was then condensed by placing the multilayer films into 105 °C for 16 h. The films were milled in a 5 vol-% APTES-anhydrous toluene solution. The excess silane was removed with ethanol, after which the centrifugation was used to obtain the desired particle size. The particles were stored in ethanol. The surface amine groups belonging to the aminopropyl moiety, were used for further modifications.

2.3. Functionalization of NPs

APTES-TCPSi functionalization to obtain APTES-TCPSi-PEG-FA was based on 1-ethyl-3-(3-dimethylaminopropyl) carbodiimide (EDC)/*N*-hydroxysuccinimide (NHS) amine crosslinking chemistry in aqueous buffer solution. To avoid unspecific crosslinking among polyethylene glycol (COOH-PEG5K-NH_2) molecules under EDC/NHS activation, the PEG-primary amine was protected via reaction with di-*tert*-butyldicarbonate $(BOC)_2O$ (Yan et al., 2017). For this, COOH-PEG-NH_2 was dissolved in dichloromethane (DCM; 2 mL), followed by addition of triethylamine (TEA) in a 1:6 M ratio (PEG:TEA), stirring in ice for 10 min. Then, $(BOC)_2O$ was added in a 1:3 M ratio [PEG:$(BOC)_2O$], stirring in ice for 30 min, and let to react overnight at room temperature (RT). Reaction mixture was dried by compressed air and the crude was dissolved in Milli-Q water, dialyzed for 24 h, and COOH-PEG-NH-BOC was obtained by lyophilization. The activation of carboxylic acid groups was allowed to occur in 12 mL of 2-(*N*-morpholino)ethanesulfonic acid (MES) buffer (pH 5.2) with 24 mg (0.1 mmol) of NHS and 31.98 μL (0.2 mmol) of EDC, at 300 rpm, for 90 min, protected from light. APTES-TCPSi NPs (6 mg) were dispersed in the previously prepared solution of activated COOH-PEG-NH_2-BOC, with a final ratio of 1.5:1 (w/w) (polymer:NPs). APTES-TCPSi-PEG-NH-BOC NPs were rinsed with Milli-Q water followed by ethanol with intercalated centrifugations. The BOC group was removed by adding DCM (3 mL) and trifluoracetic acid (1 mL) (Lundt et al., 1978), stirred for 30 min in ice, dried, washed with ethanol and Milli-Q water. As final step, APTES-TCPSi-PEG-NH_2 NPs were added to a previously prepared solution of activated FA (EDC/NHS crosslinking reaction as described above) with a final ratio of 1.5:1 (w/w) (ligand:NPs). NPs were rinsed, centrifuged and stored in Milli-Q water at 1.5 mg/mL, at 4 °C, for further experiments.

2.4. Physicochemical characterization of NPs

2.4.1. Pore volume and diameter, and specific surface area of unmodified NPs

The porous structure of the nanoparticles was analyzed with nitrogen sorption at − 196 °C using TriStar 3000 instrument (Micromeritics Inc., USA) (Bimbo et al., 2010; Makila et al., 2012).

2.4.2. Size, dispersity, surface charge and surface chemistry of NPs

The functionalization success of NPs was confirmed through different methods by comparing APTES-TCPSi-PEG-FA with APTES-TCPSi, as follows: hydrodynamic diameter (Z-average), polydispersity index (PdI) and zeta (ζ)-potential of NPs dispersed in Milli-Q water, at 10 μg/mL, were characterized by dynamic and electrophoretic light scattering (DLS and ELS) using a Zetasizer Nano ZS (Malvern Instruments Ltd, Malvern, UK). NP size and morphology were also investigated by transmission electron microscopy (TEM). Droplets of NP suspension in Milli-Q water were placed on top of carbon-coated copper TEM grids and dried at RT. Micrographs were recorded using JEM-1400 transmission electron microscope (JEOL Ltd., Tokyo, Japan) operating at 80 kV. NP functionalization was also analyzed using Fourier transform infrared (FTIR) spectroscopy. KBr pellets were prepared with 1 mg of lyophilized NP samples and analyzed using a Nicolet iS10 spectrometer (ThermoFisher Scientific, Waltham, MA, USA) with Smart OMNI-Transmission accessory. FTIR spectra were recorded using a resolution of 4 cm^{-1} at RT using OMNIC™ 8.3 software (ThermoFisher Scientific).

2.5. LEM2 loading into NPs

Drug loading was performed by the immersion method (Salonen et al., 2008). APTES-TCPSi or APTES-TCPSi-PEG-FA NPs (200 μg) were dispersed and immersed in 250 μL of LEM2 solution in dichloroethane (DCE) at 5 mg/mL with stirring at 300 rpm for 2 h, protected from light at RT. Loaded NPs were collected by centrifugation at 16,110*g* for 10 min and washed with 50 μL of ethanol to remove the excess of unloaded drug and DCE remains. Loaded NPs were then dispersed in 1 mL of DCE and stirred for 1 h, protected from light. After that, NPs were centrifuged and the amount of LEM2 in the supernatant was analyzed using high-performance liquid chromatography (HPLC, Agilent 1 260, Agilent Technologies, Santa Clara, CA, USA). The HPLC method was established using a C18 column (4.6 × 150 mm, 5 μm, Supelco Discovery, USA) with a mobile phase of methanol/water (70:30) in isocratic system, at RT. The injected volume was 20 μL, the flow rate was 0.7 mL/min, and the absorbance was measured at 240 nm wavelength. A calibration curve of LEM2 (0.047–48.5 μg/mL) in DCE was established in triplicate, and the quantification of LEM2 was based on the total area under the curve (Supplementary material, Fig. S1). The loading degree, LD (%), and encapsulation efficiency, EE (%), were calculated based on the following Eqs. (1) and (2):

$$LD(\%) = \left(\frac{m_{\mathrm{LEM2}}}{m_{\mathrm{NPs}} + m_{\mathrm{LEM2}}}\right) \times 100 \quad (1)$$

$$EE(\%) = \left(\frac{\left(m_{\text{initial LEM2}} - \left(m_{\text{free LEM2}} + m_{\text{washed LEM2}}\right)\right)}{m_{\text{initial LEM2}}}\right) \times 100 \quad (2)$$

where m_{NPs} and m_{LEM2}, in μg, are the masses of the nanoparticles and the drug, respectively.

2.6. LEM2 release profile

LEM2 payload release study was carried out as described elsewhere (Shahbazi et al., 2015). Briefly, LEM2-loaded APTES-TCPSi or APTES-TCPSi-PEG-FA NPs (200 μg) were gently dispersed in 5 mL of 10 mM HBSS-4-(2-hydroxyethyl)-1-piperazineethanesulfonic acid (HEPES) (pH 7.4) or 10 mM HBSS-MES (pH 6.5), at 37 °C, 300 rpm, for 3 h. Aliquots of 100 μL were taken at several time-points and replaced by pre-warmed buffer solutions to maintain the release volumes. To quantify the released LEM2, samples were then centrifuged at 16,110*g* and the supernatants were analyzed using HPLC as described in Section 2.5. Bulk LEM2 (corresponding to the amount of the highest LD (%)) was dispersed in the same buffers and was used as a control.

2.7. Stability study

The stability of NPs in cancer cell culture medium was studied as described in (Bauleth-Ramos et al., 2017). For that, 100 μg of the bare APTES-TCPSi or APTES-TCPSi-PEG-FA NPs were dispersed in 750 μL of RPMI 1640 with 10% FBS, and stirred for 2 h at 37 °C. Aliquots of 100 μL were taken at several time-points and diluted in 900 μL Milli-Q water. Thereafter, the hydrodynamic diameter, PdI, and ζ-potential were analyzed by DLS and ELS using Zetasizer Nano ZS.

2.8. Human cancer cell lines

Human breast adenocarcinoma MDA-MB-231 and colon adenocarcinoma HCT116 cell lines from ATCC (Rockville, Maryland, USA) were cultured in RPMI 1640 with 10% FBS, 1% NEAA, 1% L-glutamine and 1% penicillin–streptomycin in 25 cm^2 flasks. Cells were incubated in a BB 16 gas incubator (Heraeus Instruments GmbH, Hanau, Germany) at 37 °C, 5% CO_2 and 95% relative humidity.

2.8.1. In vitro cytocompatibility and cytotoxicity studies

The cytocompatibility of bare NPs and the cytotoxicity of LEM2-loaded NPs, were assessed by CellTiter-Glo® Luminescent Cell Viability assay, as described in (Santos et al., 2010). MDA-MB-231 and HCT116 cancer cells were seeded in a 96-well microplate with flat bottom (Corning Inc. Life Sciences, New York, USA) at 5 × 10^3 cells per well. Cells were allowed to attach for 24 h at 37 °C. Bare or LEM2-loaded NPs were dispersed in a cell culturing medium and serial dilutions were

made. Cells were incubated with 100 μL of NP suspension in each well. Final concentrations of bare NPs ranged from 37.5 to 600 μg/mL. LEM2-loaded NPs' final concentration treatments corresponded to 0.3 and 0.625 μM of LEM2, accordingly with obtained LD (%). Also, serial dilutions of bulk LEM2 (stock solution at 5 mM in DMSO) were made in cell culturing medium and cells were treated with final concentrations ranging from 0.3 to 5 μM. Cell culturing medium and 1% Triton X-100 were used as controls. Treated cancer cells were incubated for 48 h at 37 °C. Afterwards, the cancer cells were washed with 10 mM HBSS-HEPES (pH 7.4), and 100 μL of the CellTiter-Glo® Luminescent Cell Viability assay reagent was added into each well to lyse the cells. The cell viability assay reagent was allowed to react for 15 min with plate shaking, protected from light. The percentage of viable cells was determined by measuring the luminescence, using a Varioskan Flash multimode reader (Thermo Fisher Scientific).

2.8.2. *In vitro NP cellular uptake study*

Evaluation of qualitative NP cellular uptake and attachment on the cell membrane was performed using TEM. To this end, 13 mm round shape coverslips were placed on the bottom of 24-well plate (Corning Inc. Life Sciences) and MDA-MB-231 and HCT116 cancer cells were seeded at 1×10^5 cells per well (500 μL) in RPMI 1640 supplemented with 10% FBS. Cells were allowed to attach for 24 h at 37 °C. Culture medium was removed and 500 μL of bare APTES-TCPSi or APTES-TCPSi-PEG-FA NPs (dispersed in 10 mM HBSS-HEPES, pH 7.4, at 50 μg/mL), or only dispersion medium (negative control), were added into each well. Treatments were performed for 3 h at 37 °C, followed by removal of NP suspension and washing the cells with 10 mM HBSS-HEPES (pH 7.4). Next, the cells were fixed with glutaraldehyde for 15 min, washed, dehydrated with ethanol and embedded in epoxy resin, followed by slicing into 60 nm thick sections. The sections were transferred on carbon-coated copper grids for TEM imaging and were analyzed. Micrographs were acquired using Jeol JEM-1400 TEM operating at the acceleration voltage of 80 kV.

2.9. *Statistical analysis*

The experiments were performed in triplicate (n = 3) and the data is presented as mean ± standard deviation (SD; in NP physicochemical characterization, stability, loading and release assays) or mean ± standard error of the mean (SEM; in cellular assays). Data were analyzed statistically by applying two-way ANOVA (cells viability assay) followed by Dunnet's multiple comparisons using the GraphPad Prism 7 software (GraphPad Software, California, USA). Considered levels of significant differences were set at probabilities $*p < 0.05$, $**p < 0.01$, and $***p < 0.001$.

3. Results

3.1. *Functionalization and physicochemical characterization of the NPs*

The core of the PSi NP used in the present work was produced by a top-down procedure (Makila et al., 2012), its surface was stabilized by thermal carbonization and followed by modification with APTES to provide amine functionalization. The obtained APTES-TCPSi NPs presented a specific surface area of 352 ± 3 m^2/g, pore volume of 0.76 ± 0.03 cm^3/g and pore diameter of 8.6 ± 0.4 nm.

Cellular membrane FR has been reported as an appealing target for anticancer targeted drug delivery by decorating the nanosystems with the natural ligand FA (Cheung et al., 2016). Herein, surface functionalization of APTES-TCPSi core with FA was designed. To this end, since FA is a small ligand, to increase the blood circulation half-time of NPs by preventing opsonization, a polymer of 5 kDa (COOH-PEG-NH_2) was added between NP and the FA (Knop et al., 2010). The aromatic amine of FA is necessary for receptor recognition (Chen et al., 2013). Therefore, PEG dually functionalized with a carboxylic acid and a primary amine was chosen to ensure the subsequent conjugation of the carboxylic acid of FA with the NH_2-terminal of PEG, which maintained the aromatic amine of FA free for interaction with the receptor. Fig. 1 A shows the design strategy of the NP functionalization. The reactions of NPs with polymer and ligand were performed using EDC/NHS crosslinking chemistry under aqueous conditions (Hermanson, 2013). Since PEG contains primary amine, its protection with BOC was necessary to avoid unspecific crosslinking during the –COOH activation.

To confirm the success of the NP functionalization with FA, ζ-potential, size, and PdI were measured using DLS and ELS (Table 1). Indeed, it was possible to identify differences in surface charge between the unmodified (APTES-TCPSi) and the modified (APTES-TCPSi-PEG-FA) NPs. The unmodified NPs presented a positive charge due to $–NH_2$/NH_3^+ groups from the APTES moiety, which shifted to negative/neutral values after FA conjugation (Table 1), since the FA aromatic amine may be in its free state (folic acid pK_a of 3.5 and 4.3) (NIH-PubChem, 2019). Regarding the PdI, the representation of the size distribution of particles, both unmodified and modified NPs were moderately polydisperse in solution (PdI $0.1 < x < 0.4$) (Table 1) (Danaei et al., 2018). Modified NPs presented slightly higher PdI values, evidencing the chemical change on the NP shell due to functionalization (Table 1).

The analysis of the newly functionalized NPs was performed by FTIR spectroscopy. Comparing the spectra of the unmodified and modified NPs with the reference spectrum of FA revealed that the NPs were successfully functionalized with FA (Fig. 1 B). The differences detected were in the fingerprint region. NPs modified with FA spectrum showed new bands at 1680 cm^{-1} (**a**; C═O secondary amide stretch), 1597 cm^{-1} (**b**; N—H amide bend), 1546–1476 cm^{-1} (**c**; C═C aromatic stretch, multiple bands), 1380 cm^{-1} (**d**; C—H CH_2 bend), and 1280 cm^{-1} (**e**; C—N amine stretch) wavelengths, which correspond to FA reference bands (Fig. 1 B) (Coates, 2006; Tonbul et al., 2021). Furthermore, TEM analysis was performed to investigate NP morphology (Fig. 1 C). In general, the appearance of unmodified and modified NPs was similar, and the size is in accordance with the values obtained by DLS.

3.2. *LEM2 loading, in vitro release profile, and stability of NPs*

After NP functionalization, it was important to investigate the amount of LEM2 (Fig. 2 A) that the NPs could carry and deliver to the target cells. For that, the LEM2 LD (%), EE (%) and payload release profile were performed. Drug loading was performed using the immersion method (Salonen et al., 2008), in which the unmodified and modified NPs were dispersed in a concentrated LEM2 solution in DCE, allowing the incorporation of the compound within the pores. The compound is loaded due to its higher affinity with the surface of NP pores than to the solvent through physical adsorption and physical confinement contributing to drug amorphization (Makila et al., 2014). Among other solvents tested (*i.e.*, ethanol, methanol, acetonitrile, DMSO, diethyl ether, *n*-hexane and ethyl acetate, data not shown), DCE showed to be the best solvent, reaching the concentration of LEM2 at 5 mg/mL. The obtained LD (%) values were 2.33 ± 0.94% and 1.99 ± 0.97% with APTES-TCPSi and APTES-TCPSi-PEG-FA, respectively. The calculated entrapment efficiency (EE (%)) was higher for both nanoparticles, 21.89 ± 8.97 % and 22.48 ± 10.94 %, respectively. The EE (%) calculation took into consideration the washing step needed to remove solvent reminiscences, after NP immersion in drug solution, to allow NP dispersity in aqueous solution for *in vitro* assays. Different factors may affect the differences observed between EE (%) and LD (%), such as, the affinity of the drug to the NP surface, hydrophobicity of the NP surface, drug solubility in the solvent and drug molecules interaction (Karavelidis et al., 2011). Interestingly, the NP surface modification did not interfere in drug loading or entrapment efficiency.

The LEM2 payload release study indicated that a pH-independent burst release of LEM2 occurred immediately within the first minutes after the NP dispersions were placed in the buffer solutions, with no significant increase in cumulative concentration of LEM2 between 0.5 h

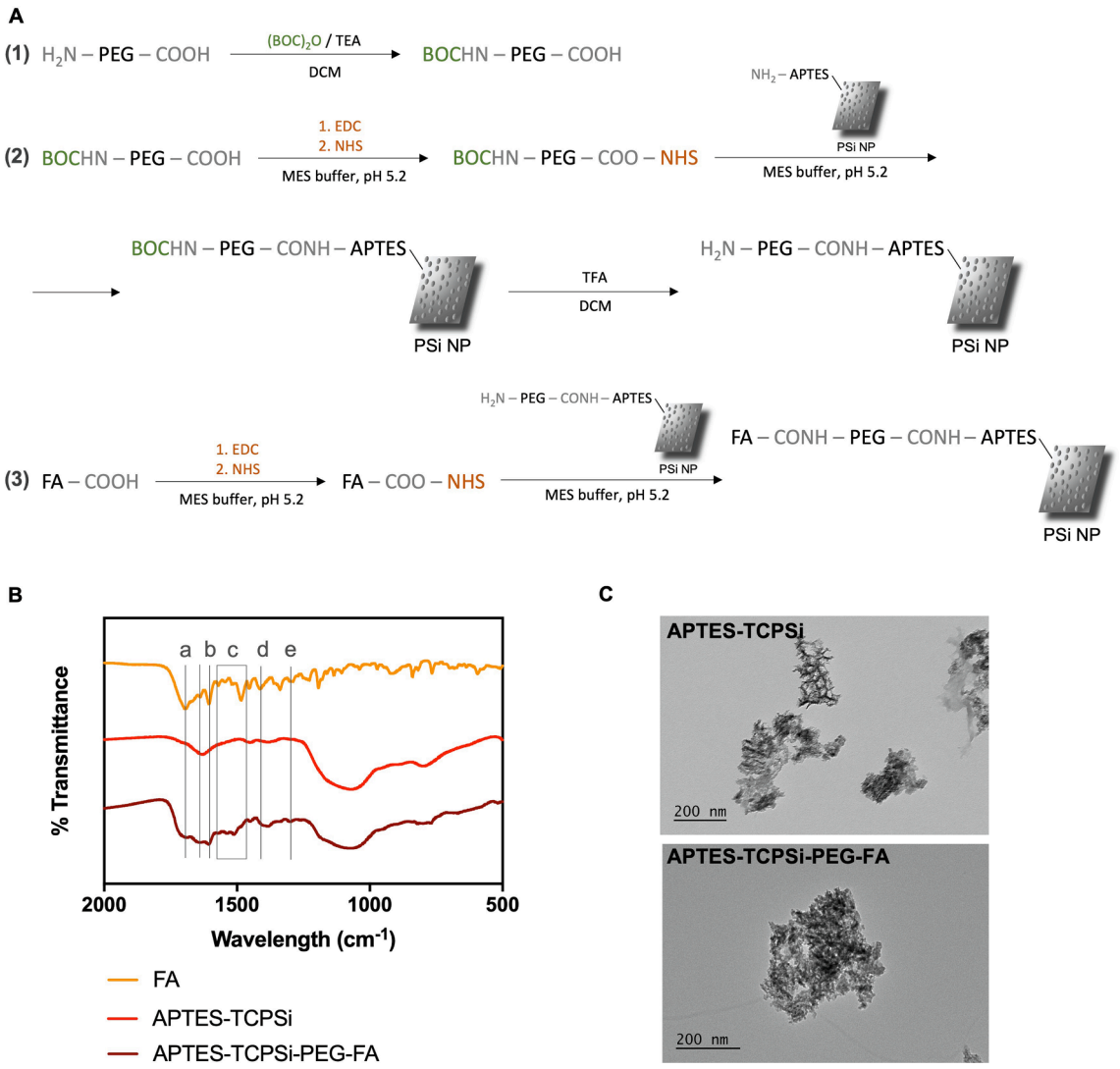

Fig. 1. NP functionalization and physicochemical characterization. (A) Chemical reaction steps of APTES-TCPSi functionalization: (1) PEG primary amine protection with $(BOC)_2O$; (2) PEG carboxylic acid activation with EDC/NHS and crosslinking reaction with APTES-TCPSi and final PEG amine deprotection; (3) FA carboxylic acid activation with EDC/NHS and crosslinking reaction with APTES-TCPSi-PEG. (B) FTIR spectra of unmodified and modified NPs and FA in KBr pellets. Bands of modified NPs that appear, change in intensity, or are shifted due to chemical modification (comparing to unmodified NPs) are highlighted and labeled a-e. (C) TEM images of unmodified and modified NPs.

Table 1
The ζ-potential, size, and PdI of unmodified and modified NPs.

	APTES-TCPSi	APTES-TCPSi-PEG-FA
ζ-potential (mV)	16.0 ± 0.7	−5.7 ± 16.5
Size average (d. nm)	332. ± 8	333 ± 94
PdI	0.19 ± 0.03	0.26 ± 0.07

Presented data are mean ± SD (n = 3).

and 3 h (Fig. 2 B). Additionally, the concentration of LEM2 remained constant between 3 h and 24 h with no detection of drug degradation (data not shown). On the contrary, bulk LEM2 in its crystalline form remained undetectable throughout the experiment up to 3 h, due to its low solubility/dissolution rate in aqueous solution, being detectable only at 24 h at concentrations lower than the lowest concentration of the calibration curve (<0.047 μg/mL, Supplementary material, Fig. S1). Although the same LEM2 payload release profiles were obtained both at pH 7.4 and 6.5, for unmodified and modified NPs, higher release was obtained for APTES-TCPSi-PEG-FA (>90%) than for APTES-TCPSi (20 to 30%) (Fig. 2 B). Although the obtained LDs (%) were low comparing to other drug payloads (Prestidge et al., 2007), the results obtained in the release studies were promising, as they indicated an improvement in LEM2 solubility.

Next, the NP stability in cell culture medium was assessed. The ζ-potential, size, and PdI of NPs were measured for 2 h, in RPMI 1640 supplemented with 10% FBS at 37 °C. NPs were shown to be stable throughout the experiment, with no surface charge alteration (constant ζ-potential) or aggregation, with unchanged size average and PdI (Fig. 2 C). This evidence showed that the NP stability in cell culture medium was suitable for further *in vitro* studies using cancer cells.

3.3. *In vitro bare NP cytocompatibility, LEM2-loaded NP cytotoxicity and uptake studies*

Bare NPs cytocompatibility and LEM2-loaded NPs cytotoxicity was evaluated by cell viability based on quantification of the total amount of ATP of metabolically active cells (Crouch et al., 1993). HCT116 and MDA-MB-231 cancer cells were chosen due to the known cytotoxicity of LEM2 against these cells (Gomes et al., 2019), and due to their over-expression of FR (Chen et al., 2012). Bare NPs were analyzed to

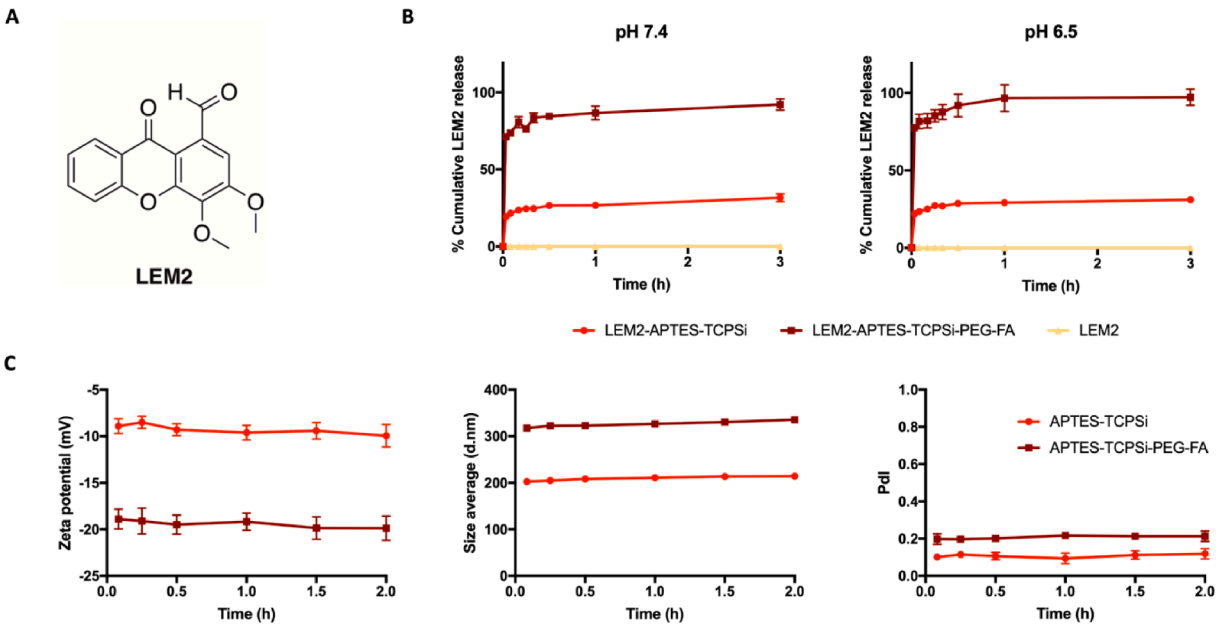

Fig. 2. Release profile of LEM2-loaded NPs and stability of bare NPs. (A) LEM2, 1-carbaldehyde-3,4-dimethoxy-9*H*-xanthen-9-one, chemical structure. (B) Release profiles of LEM2-loaded modified and unmodified NPs (200 μg) in 5 mL of HBSS-HEPES (pH 7.4, simulating the physiological pH) and HBSS-MES (pH 6.5, simulating the pH in tumor microenvironment) during 3 h, at 37 °C. Bulk LEM2 (in the same amount of LEM2 loaded in NPs calculated based on the highest LD (%)) was used as control. The amount of LEM2 released is presented in cumulative % and data are mean ± SD (n = 3). (C) Bare NPs (100 μg) stability in 750 μL of RPMI 1640 with 10% FBS culture medium during 2 h, at 37 °C, was assessed by ζ-potential, size average and PdI. Presented data are mean ± SD (n = 3).

investigate whether they could be *per se* cytotoxic against these human cancer cells. To determine the highest non-toxic concentration of bare NPs, cells were treated with a NP concentration ranging from 37.5 to 600 μg/mL. The concentration range of NPs was chosen considering two concentrations above and two concentrations below 150 μg/mL (this value corresponds to the amount of bare NPs required to attain 5 μM LEM2, according to the lowest LD (%)). The results showed that unmodified and modified NPs exhibited a concentration-dependent cytotoxic effect in both cancer cell lines. In general, NPs revealed to be cytotoxic at the highest concentrations (150, 300, and 600 μg/mL), with cell viability lower than 60% in both cancer cell lines (Fig. 3 A). In general, the two lowest NP concentrations of 37.5 and 75 μg/mL showed to be cytocompatible, with cell viability values higher than 90% in both tested cancer cell lines (Fig. 3 A).

Thereafter, cancer cells were treated with bulk LEM2 and LEM2-loaded NPs, with two concentrations of LEM2, 0.3 and 0.625 μM, for which bulk LEM2 had no cytotoxicity (Fig. 3 B). The amount of NPs was adjusted to both LEM2 concentrations for cell treatment, according to previously obtained LD (%), corresponding to NPs concentrations ranging from 3.7 to 8.9 μg/mL. Of note, these NP amounts were lower than the lowest concentration of NPs tested with no impact on cell viability (37.5 μg/mL, Fig. 3 A). LEM2-loaded APTES-TCPSi-PEG-FA NPs increased LEM2 cytotoxicity at both concentrations tested of LEM2, by reducing the viability of both cancer cell lines (Fig. 3 C). In HCT116 cancer cells, LEM2-loaded APTES-TCPSi-PEG-FA NPs, at 0.3 and 0.625 μM, revealed to induce a significant reduction of cell viability (21.0 ± 12.7% and 11.9 ± 4.3%, respectively) compared to bulk LEM2 (Fig. 3 C). MDA-MB-231 cancer cells showed to be less sensitive to LEM2 cytotoxicity (Fig. 3 B, C). Nevertheless, a similar profile was observed in MDA-MB-231 cancer cells with a significant reduction of cell viability for both concentrations of LEM2-loaded APTES-TCPSi-PEG-FA NPs (46.8 ± 2.2% at 0.3 μM and 30.8 ± 2.4% at 0.625 μM) (Fig. 3 C).

It was also relevant to investigate if the modified NPs were uptaken by cancer cells within the first hours of cell treatment. For this, cells were treated with bare unmodified and modified NPs and analyzed by TEM. TEM micrographs showed that both NPs were associated with cell membranes and uptaken by HCT116 and MDA-MB-231 cancer cells, being confined in large vesicles (with the size varying roughly from 200 to 1000 nm) within the cell cytoplasm (Fig. 4). In addition, it became evident that some cells presented plasma membrane protrusions next to NPs, as observed in APTES-TCPSi-PEG-FA treatment in both cancer cell lines (Fig. 4, red arrows).

4. Discussion

Herein, PSi-based nanosystems were developed to overcome LEM2 low solubility to enable further *in vivo* studies. In general, PSi NPs improve the solubility of poorly water-soluble drugs, reduce the pH-dependency of the dissolution process, and the release is based on faster diffusion than the bulk drug (Santos et al., 2014).

The functionalization of APTES-TCPSi NPs with PEG and FA succeeded well with the preparation of APTES-TCPSi-PEG-FA NPs using the EDC/NHS crosslinking chemistry approach (Hermanson, 2013). LEM2 was loaded into the NPs by immersion, a simple and convenient method, despite the low loading efficiency associated with this method (Li et al., 2018; Salonen et al., 2008). In the immersion method, drug loading occurs mainly by physical adsorption of the drug molecules on the surface of PSi NP pores (Hillerström et al., 2014). Although high LD (%) of drug payload can be achieved with PSi due to high porosity/pore volume (Li et al., 2018), herein the obtained LD (%) was low. The obtained EE (%) was higher than the LD (%). This can be attributed to a higher affinity of LEM2 to the solvent than to the PSi, or to relatively low concentration of the compound in solution (Salonen et al., 2008). Despite this, it was not possible to obtain higher LD (%) with other solvents, such as DMSO or acetonitrile, in which LEM2 solubility is lower. As such, DCE rendered the best LD (%).

The payload release profile indicated that LEM2 was burst released, which is in line with PSi NPs without sealed pores (Li et al., 2018; Makila et al., 2014). This indicated that the unmodified and the modified NPs increased the solubility and dissolution rate of LEM2 in aqueous buffers when compared to undetectable amounts of bulk LEM2, suggesting that drug amorphization could be taking place (Hancock and Zografi, 1997). Interestingly, APTES-TCPSi NPs presented lower drug release than APTES-TCPSi-PEG-FA. Lower drug release may be attributable to the

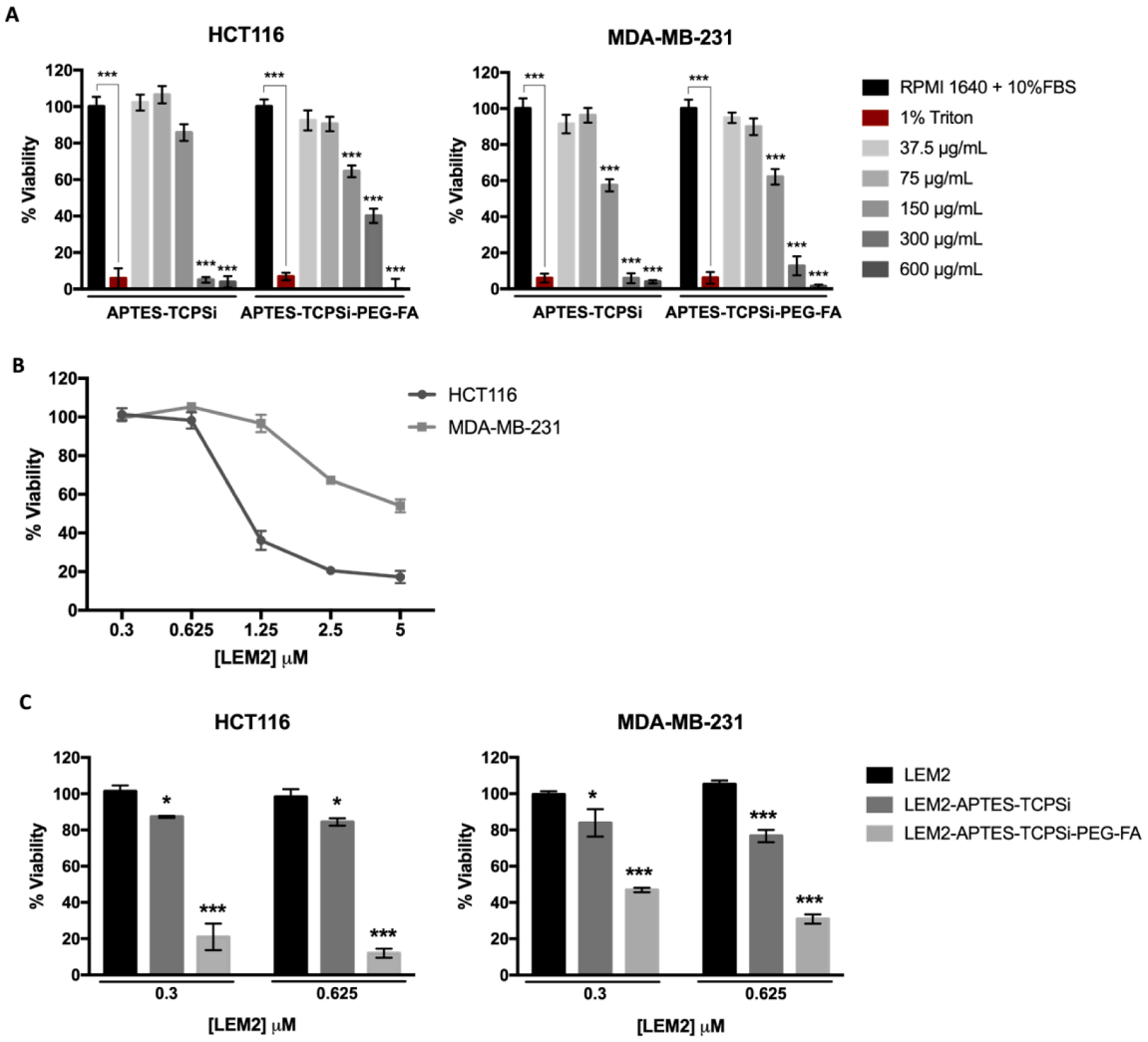

Fig. 3. Bare NPs are cytocompatible at lower concentrations and LEM2-loaded modified NPs increase LEM2 cytotoxicity in human cancer cells. Cell viability in HCT116 and MDA-MB-231 cancer cells was evaluated after co-incubation with (A) bare NPs (37.5–600 μg/mL), (B) bulk LEM2 (0.3 to 5 μM), or (C) LEM2-loaded NPs, for 48 h. Cells treated with RPMI 1640 with 10% FBS or 1% Triton X-100 were used as negative and positive controls, respectively. The amount of LEM2-loaded NPs was calculated through LD (%), to treat cells with the same amount of NP-loaded LEM2 corresponding to bulk LEM2 concentrations of 0.3 and 0.625 μM. Treatment with bulk LEM2 was used as a negative control at the same concentrations. Presented data are mean ± SEM (n = 3). Significant differences between means (negative control *vs* NPs treatments) were statistically analyzed by two-way ANOVA with Dunnet's multiple comparisons test (*$p < 0.05$, **$p < 0.01$, and ***$p < 0.001$).

retention of a portion of the drug inside PSi NPs by the establishment of stronger interactions between the cargo molecules and the PSi surface, or due to small crystalline nuclei of drug blocking the pores (McCarthy et al., 2018). However, in this case, the lower LEM2 release observed with APTES-TCPSi NPs can be associated with problems in drug loading, as the immersion method can have reproducibility problems (Salonen et al., 2008), rather than to the establishment of covalent bonds among LEM2 aldehyde group and APTES-TCPSi primary amines, since loading occurs under catalyst-free organic solvent at RT and normal pressure. Of note is that the pH showed not to be a critical factor in LEM2 release as expected (Santos et al., 2014), showing that the LEM2 payload release is adequate in physiological pH and tumor microenvironment. Additionally, NPs were found to be stable in cell culture medium, maintaining their dispersity, an important factor for cancer cell treatment.

The NPs developed herein exhibited concentration-dependent cytotoxicity, as demonstrated with PSi NPs in other studies (Bimbo et al., 2012; Sarparanta et al., 2012) and are cytocompatible in cancer cells at concentrations lower than 75 μg/mL. LEM2-loaded NPs increased LEM2 cytotoxicity by improving its solubility and delivering it intracellularly. Indeed, LEM2-loaded NPs significantly decreased cancer cell viability compared to bulk LEM2 at the same tested concentrations, with no NP-associated cytotoxicity (NP concentrations were lower than the lowest cytocompatible tested concentration). Of note is that cytotoxic selectivity was evident among the LEM2-loaded modified and unmodified NPs, with a stronger cytotoxic effect with APTES-TCPSi-PEG-FA NPs treatment. As such, the observed cytotoxic selectivity could be associated with the lower cumulative release of the LEM2-loaded unmodified NPs or with the FR-targeted cellular uptake by FA. Cellular membrane FR is associated with the selective NP internalization via ligand-receptor mediated endocytosis (Langston Suen and Chau, 2014). Several studies have reported that the active targeting of mesoporous silica NPs with FA is a successful strategy, by being selectively uptaken by cells and increasing the potency of the carried drug comparing to unmodified NPs (Chen et al., 2018; Porta et al., 2013; Tonbul et al., 2021). Therefore, NP cellular uptake was investigated and was confirmed for 3 h of treatment, but no evident cellular uptake selectivity was observed for the time tested. Interestingly, Porta *et al.* reported that the selective uptake of FA-NPs, by human cells, occurred at 6 h treatment, and Tonbul *et al.* observed the uptake difference at 2 h or 4 h, depending on the cell line (Porta et al., 2013; Tonbul et al., 2021). Therefore, a kinetic uptake

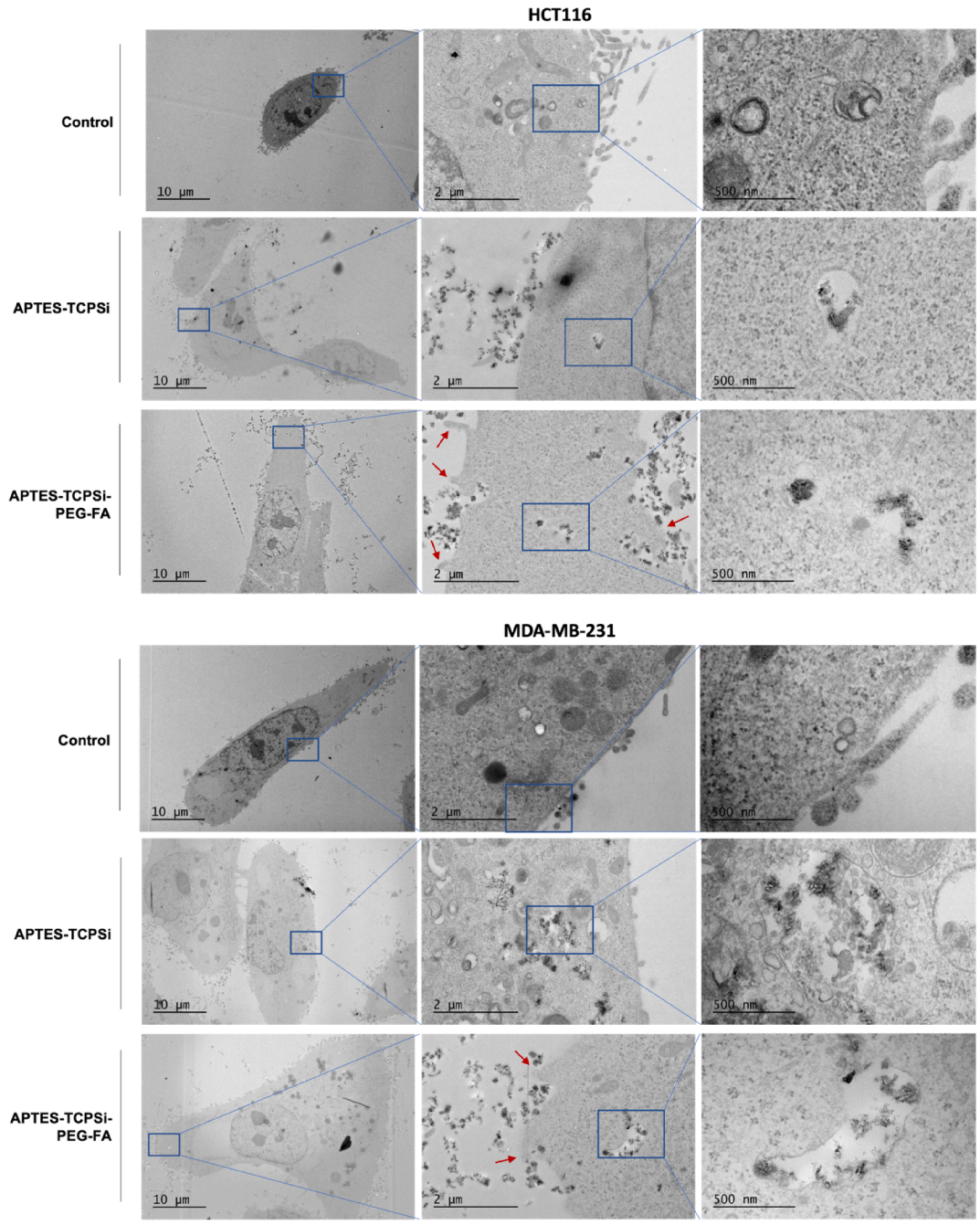

Fig. 4. Modified and unmodified NPs are uptaken by cancer cells. TEM micrographs show NP internalization by HCT116 and MDA-MB-231 cancer cells after 3 h treatment with modified and unmodified bare NPs at 50 µg/mL. Cell culture medium was used as negative control. Red arrows identify cellular protusions. From left to right, the magnifications are as follows: first micrograph 500×, second micrograph 4000×, and third micrograph 15,000×. The micrographs were recorded at an acceleration voltage of 80 kV. (For interpretation of the references to colour in this figure legend, the reader is referred to the web version of this article.)

study of the NPs developed in our work should be pursued. It was also hypothesized that modified NPs could be internalized by both selective and non-selective mechanisms, whereas unmodified NPs would be internalized by non-selective mechanisms. The large intracellular vesicles containing NPs and plasma membrane protrusions observed by TEM, as well as the NP size around 330 nm, raises the possibility that macropinocytosis could also occur (Behzadi et al., 2017). Therefore, further uptake studies should be performed to better elucidate the uptake pathway of these NPs, in these cancer cells.

PSi matrix exhibits biodegradability, by dissolving into orthosilicates, which rate is tuned by different factors, such as size, porosity, morphology, surface chemistry, functionalization and medium/environment conditions (Croissant et al., 2017). Specifically, bigger pores favor PSi dissolution than smaller ones (Martinez et al., 2013), thermally carbonized NPs showed to resist longer to biodegradation than oxidized ones (Kovalainen et al., 2018) and functionalization with PEG(5k) also prolonged the time of PSi dissolution (Godin et al., 2010). Regarding the environment conditions, PSi dissolution is favored in alkaline pH and presence of solubilizing nucleophilic species (Croissant et al., 2017). Therefore, APTES-TCPSi-PEG-FA are expected to take some weeks to fully dissolve. Regarding *in vivo* settings, several works have been done, highlighting that PSi NPs had the ability to accumulate in the spleen and in the liver, and then were cleared over time (Tanaka et al., 2010b; Tzur-Balter et al., 2015). Also, PSi-based NPs *in vivo* safety doses

and maximum tolerated doses have been reported (Nishimori et al., 2009; Tanaka et al., 2010a; Yu et al., 2012) and to the interest of the present work, the obtained LEM2 loading degree should be optimized in APTES-TCPSI-PEG-FA to allow the administration of a NP dose bellow the described concentrations (100 mg/kg).

Altogether, both the APTES-TCPSi and APTES-TCPSi-PEG-FA NPs showed to be cytocompatible in cancer cells, improved LEM2 solubility and cytotoxicity. LEM2-loaded APTES-TCPSi-PEG-FA NPs showed to be more effective in enhancing the LEM2 anticancer activity and bioavailability. Hence, the developed LEM2-folate decorated mesoporous silicon nanodelivery system, described herein, paves new opportunities envisioning an optimized nanoformulation to pursue LEM2 *in vivo* studies.

CRediT authorship contribution statement

Ana Sara Gomes: Conceptualization, Investigation, Methodology, Validation, Formal analysis, Visualization, Writing – original draft, Writing – review & editing. **Alexandra Correia:** Investigation, Validation, Writing – review & editing. **Antti Rahikkala:** Investigation, Writing – review & editing. **Ermei Mäkilä:** Resources, Writing – review & editing. **Madalena M. Pinto:** Writing – review & editing. **Emília Sousa:** Resources, Supervision, Writing – review & editing. **Jarno Salonen:** Resources. **Lucília Saraiva:** Conceptualization, Supervision, Writing – review & editing. **Hélder A. Santos:** Conceptualization, Supervision, Resources, Project administration, Funding acquisition, Writing – review & editing.

Declaration of Competing Interest

The authors declare that they have no known competing financial interests or personal relationships that could have appeared to influence the work reported in this paper.

Acknowledgement

This research was supported by national funds through FCT (Foundation for Science and Technology) within the scope of UIDB/04423/2020, UIDP/04423/2020 and UIDB/50006/2020. We also thank FCT for the financial support through fellowships PD/BD/114046/2015 (A. S. Gomes), and the Programa Operacional Potencial Humano (POCH), specifically the BiotechHealth Programme (PD/00016/2012). Prof. H. A. Santos acknowledges financial support from the Sigrid Jusélius Foundation, the Academy of Finland (grant no. 331151), and the UMCG Research Funds. We thank Electron Microscopy Unit of the Institute of Biotechnology, University of Helsinki.

Appendix A. Supplementary material

Supplementary data to this article can be found online at https://doi.org/10.1016/j.ijpharm.2022.121959.

References

Amidon, G.L., Lennernas, H., Shah, V.P., Crison, J.R., 1995. A theoretical basis for a biopharmaceutic drug classification: the correlation of in vitro drug product dissolution and in vivo bioavailability. Pharm. Res. 12, 413–420.
Anglin, E., Cheng, L., Freeman, W., Sailor, M., 2008. Porous silicon in drug delivery devices and materials. Adv. Drug Deliv. Rev. 60 (11), 1266–1277.
Bauleth-Ramos, T., Shahbazi, M.A., Liu, D., Fontana, F., Correia, A., Figueiredo, P., Zhang, H., Martins, J.P., Hirvonen, J.T., Granja, P., Sarmento, B., Santos, H.A., 2017. Nutlin-3a and Cytokine Co-loaded Spermine-Modi ed Acetalated Dextran Nanoparticles for Cancer Chemo-Immunotherapy. Adv. Funct. Mater. 27, 1703303.
Behzadi, S., Serpooshan, V., Tao, W., Hamaly, M.A., Alkawareek, M.Y., Dreaden, E.C., Brown, D., Alkilany, A.M., Farokhzad, O.C., Mahmoudi, M., 2017. Cellular uptake of nanoparticles: journey inside the cell. Chem. Soc. Rev. 46 (14), 4218–4244.
Bimbo, L.M., Sarparanta, M., Makila, E., Laaksonen, T., Laaksonen, P., Salonen, J., Linder, M.B., Hirvonen, J., Airaksinen, A.J., Santos, H.A., 2012. Cellular interactions of surface modified nanoporous silicon particles. Nanoscale 4, 3184–3192.
Bimbo, L.M., Sarparanta, M., Santos, H.A., Airaksinen, A.J., Makila, E., Laaksonen, T., Peltonen, L., Lehto, V.P., Hirvonen, J., Salonen, J., 2010. Biocompatibility of thermally hydrocarbonized porous silicon nanoparticles and their biodistribution in rats. ACS Nano 4, 3023–3032.
Candi, E., Agostini, M., Melino, G., Bernassola, F., 2014. How the TP53 family proteins TP63 and TP73 contribute to tumorigenesis: regulators and effectors. Hum. Mutat. 35, 702–714.
Chen, C., Ke, J., Zhou, X.E., Yi, W., Brunzelle, J.S., Li, J., Yong, E.L., Xu, H.E., Melcher, K., 2013. Structural basis for molecular recognition of folic acid by folate receptors. Nature 500, 486–489.
Chen, H., Li, S., Li, B., Ren, X., Li, S., Mahounga, D.M., Cui, S., Gu, Y., Achilefu, S., 2012. Folate-modified gold nanoclusters as near-infrared fluorescent probes for tumor imaging and therapy. Nanoscale 4, 6050–6064.
Chen, X., Liu, Y., Lin, A., Huang, N., Long, L., Gang, Y., Liu, J., 2018. Folic acid-modified mesoporous silica nanoparticles with pH-responsiveness loaded with Amp for an enhanced effect against anti-drug-resistant bacteria by overcoming efflux pump systems. Biomater. Sci. 6, 1923–1935.
Cheung, A., Bax, H.J., Josephs, D.H., Ilieva, K.M., Pellizzari, G., Opzoomer, J., Bloomfield, J., Fittall, M., Grigoriadis, A., Figini, M., Canevari, S., Spicer, J.F., Tutt, A.N., Karagiannis, S.N., 2016. Targeting folate receptor alpha for cancer treatment. Oncotarget 7, 52553–52574.
Coates, J., 2006. Interpretation of Infrared Spectra, A Practical Approach. In: Meyers, R. A. (Ed.), Encyclopedia of Analytical Chemistry. John Wiley & Sons Ltd.
Croissant, J.G., Fatieiev, Y., Khashab, N.M., 2017. Degradability and Clearance of Silicon, Organosilica, Silsesquioxane, Silica Mixed Oxide, and Mesoporous Silica Nanoparticles. Adv. Mater. 29 (9), 1604634.
Council of Europe, 2022. European Pharmacopoeia: General notices 10 (8), 7.
Crouch, S.P.M., Kozlowski, R., Slater, K.J., Fletcher, J., 1993. The use of ATP bioluminescence as a measure of cell proliferation and cytotoxicity. J. Immunol. Methods 160, 81–88.
Danaei, M., Dehghankhold, M., Ataei, S., Hasanzadeh Davarani, F., Javanmard, R., Dokhani, A., Khorasani, S., Mozafari, M.R., 2018. Impact of Particle Size and Polydispersity Index on the Clinical Applications of Lipidic Nanocarrier Systems. Pharmaceutics 10 (2), 57.
Din, F.U., Aman, W., Ullah, I., Qureshi, O.S., Mustapha, O., Shafique, S., Zeb, A., 2017. Effective use of nanocarriers as drug delivery systems for the treatment of selected tumors. Int. J. Nanomedicine 12, 7291–7309.
Godin, B., Gu, J., Serda, R.E., Bhavane, R., Tasciotti, E., Chiappini, C., Liu, X., Tanaka, T., Decuzzi, P., Ferrari, M., 2010. Tailoring the degradation kinetics of mesoporous silicon structures through PEGylation. J. Biomed. Mater. Res. A 94, 1236–1243.
Gomes, A.S., Ramos, H., Inga, A., Sousa, E., Saraiva, L., 2021. Structural and Drug Targeting Insights on Mutant p53. Cancers 13, 3344.
Gomes, S., Raimundo, L., Soares, J., Loureiro, J.B., Leao, M., Ramos, H., Monteiro, M.N., Lemos, A., Moreira, J., Pinto, M., Chlapek, P., Veselska, R., Sousa, E., Saraiva, L., 2019. New inhibitor of the TAp73 interaction with MDM2 and mutant p53 with promising antitumor activity against neuroblastoma. Cancer Lett. 446, 90–102.
Hancock, B.C., Parks, M., 2000. What is the true solubility advantage for amorphous pharmaceuticals? Pharm. Res. 17, 397–404.
Hancock, B.C., Zografi, G., 1997. Characteristics and significance of the amorphous state in pharmaceutical systems. J. Pharm. Sci. 86, 1–12.
Hermanson, G.T., 2013. Chapter 3 - The Reactions of Bioconjugation. Elsevier Inc, Bioconjugate Techniques.
Hillerström, A., Andersson, M., Samuelsson, J., Stam, J., 2014. Solvent strategies for loading and release in mesoporous silica. Colloids Interface Sci. Commun. 3, 5–8.
Hon, N.K., Shaposhnik, Z., Diebold, E.D., Tamanoi, F., Jalali, B., 2012. Tailoring the biodegradability of porous silicon nanoparticles. J. Biomed. Mater. Res. A 100, 3416–3421.
Karavelidis, V., Karavas, E., Giliopoulos, D., Papadimitriou, S., Bikiaris, D., 2011. Evaluating the effects of crystallinity in new biocompatible polyester nanocarriers on drug release behavior. Int. J. Nanomedicine 6, 3021–3032.
Knop, K., Hoogenboom, R., Fischer, D., Schubert, U.S., 2010. Poly(ethylene glycol) in drug delivery: pros and cons as well as potential alternatives. Angew. Chem. Int. Ed. Engl. 49, 6288–6308.
Kovalainen, M., Kamakura, R., Riikonen, J., Finnila, M., Nissinen, T., Rantanen, J., Niemela, M., Peramaki, P., Makinen, M., Herzig, K.H., Lehto, V.P., 2018. Biodegradation of inorganic drug delivery systems in subcutaneous conditions. Eur. J. Pharm. Biopharm. 122, 113–125.
Langston Suen, W.L., Chau, Y., 2014. Size-dependent internalisation of folate-decorated nanoparticles via the pathways of clathrin and caveolae-mediated endocytosis in ARPE-19 cells. J. Pharm. Pharmacol. 66, 564–573.
Li, W., Liu, Z., Fontana, F., Ding, Y., Liu, D., Hirvonen, J.T., Santos, H.A., 2018. Tailoring Porous Silicon for Biomedical Applications: From Drug Delivery to Cancer Immunotherapy. Adv. Mater. 30, e1703740.
Lipinski, C., 2002. Poor aqueous solubility - an industry wide problem in drug discovery. Am. Pharm. Rev. 5, 82–85.
Lundt, B.F., Johansen, N.L., Volund, A., Markussen, J., 1978. Removal of t-butyl and t-butoxycarbonyl protecting groups with trifluoroacetic acid. Mechanisms, biproduct formation and evaluation of scavengers. Int. J. Pept. Protein Res. 12, 258–268.
Makila, E., Bimbo, L.M., Kaasalainen, M., Herranz, B., Airaksinen, A.J., Heinonen, M., Kukk, E., Hirvonen, J., Santos, H.A., Salonen, J., 2012. Amine modification of thermally carbonized porous silicon with silane coupling chemistry. Langmuir 28, 14045–14054.
Makila, E., Ferreira, M.P., Kivela, H., Niemi, S.M., Correia, A., Shahbazi, M.A., Kauppila, J., Hirvonen, J., Santos, H.A., Salonen, J., 2014. Confinement effects on drugs in thermally hydrocarbonized porous silicon. Langmuir 30, 2196–2205.

Malta, R., Loureiro, J.B., Costa, P., Sousa, E., Pinto, M., Saraiva, L., Amaral, M.H., 2021. Development of lipid nanoparticles containing the xanthone LEM2 for topical treatment of melanoma. J. Drug Delivery Sci. Technol. 61, 1–9.

Martinez, J.O., Chiappini, C., Ziemys, A., Faust, A.M., Kojic, M., Liu, X., Ferrari, M., Tasciotti, E., 2013. Engineering multi-stage nanovectors for controlled degradation and tunable release kinetics. Biomaterials 34, 8469–8477.

McCarthy, C.A., Ahern, R.J., Devine, K.J., Crean, A.M., 2018. Role of Drug Adsorption onto the Silica Surface in Drug Release from Mesoporous Silica Systems. Mol. Pharm. 15, 141–149.

Mirza, A.Z.S.F.A., 2014. Nanomedicine and drug delivery: a mini review. Int. Nano Lett. 4, 1–7.

Misra, R., Acharya, S., Sahoo, S.K., 2010. Cancer nanotechnology: application of nanotechnology in cancer therapy. Drug Discov. Today 15, 842–850.

NIH-PubChem, 2019. Folic acid (compound).

Nishimori, H., Kondoh, M., Isoda, K., Tsunoda, S., Tsutsumi, Y., Yagi, K., 2009. Silica nanoparticles as hepatotoxicants. Eur. J. Pharm. Biopharm. 72, 496–501.

Patra, J.K., Das, G., Fraceto, L.F., Campos, E.V.R., Rodriguez-Torres, M.D.P., Acosta-Torres, L.S., Diaz-Torres, L.A., Grillo, R., Swamy, M.K., Sharma, S., Habtemariam, S., Shin, H.S., 2018. Nano based drug delivery systems: recent developments and future prospects. J. Nanobiotechnol. 16, 71.

Porta, F., Lamers, G.E., Morrhayim, J., Chatzopoulou, A., Schaaf, M., den Dulk, H., Backendorf, C., Zink, J.I., Kros, A., 2013. Folic acid-modified mesoporous silica nanoparticles for cellular and nuclear targeted drug delivery. Adv. Healthc. Mater. 2, 281–286.

Prestidge, C.A., Barnes, T.J., Lau, C.H., Barnett, C., Loni, A., Canham, L., 2007. Mesoporous silicon: a platform for the delivery of therapeutics. Expert Opin. Drug Deliv. 4, 101–110.

Ramos, H., Raimundo, L., Saraiva, L., 2020. p73: From the p53 shadow to a major pharmacological target in anticancer therapy. Pharmacol. Res. 162, 105245.

Rosenholm, J.M., Mamaeva, V., Sahlgren, C., Linden, M., 2012. Nanoparticles in targeted cancer therapy: mesoporous silica nanoparticles entering preclinical development stage. Nanomedicine (Lond) 7, 111–120.

Salonen, J., Kaukonen, A.M., Hirvonen, J., Lehto, V.P., 2008. Mesoporous silicon in drug delivery applications. J. Pharm. Sci. 97, 632–653.

Salonen, J.L., Lehto, V.P., 2008. Fabrication and chemical surface modification of mesoporous silicon for biomedical applications. Chem. Eng. J. 137, 162–172.

Santos, H.A., Makila, E., Airaksinen, A.J., Bimbo, L.M., Hirvonen, J., 2014. Porous silicon nanoparticles for nanomedicine: preparation and biomedical applications. Nanomedicine (Lond) 9, 535–554.

Santos, H.A., Riikonen, J., Salonen, J., Makila, E., Heikkila, T., Laaksonen, T., Peltonen, L., Lehto, V.P., Hirvonen, J., 2010. In vitro cytotoxicity of porous silicon microparticles: effect of the particle concentration, surface chemistry and size. Acta Biomater. 6, 2721–2731.

Sarparanta, M., Bimbo, L.M., Rytkonen, J., Makila, E., Laaksonen, T.J., Laaksonen, P., Nyman, M., Salonen, J., Linder, M.B., Hirvonen, J., Santos, H.A., Airaksinen, A.J., 2012. Intravenous delivery of hydrophobin-functionalized porous silicon nanoparticles: stability, plasma protein adsorption and biodistribution. Mol. Pharm. 9, 654–663.

Shahbazi, M.A., Herranz, B., Santos, H.A., 2012. Nanostructured porous Si-based nanoparticles for targeted drug delivery. Biomatter 2, 296–312.

Shahbazi, M.A., Shrestha, N., Mäkilä, E., Araújo, F., Correia, A., Ramos, T., Sarmento, B., Salonen, J., Hirvonen, J., Santos, H.A., 2015. A prospective cancer chemo-immunotherapy approach mediated by synergistic CD326 targeted porous silicon nanovectors. Nano Res. 8, 1505–1521.

Sing, K.S.W., Everett, D.H., Haul, R.A.W., Moscou, L., Pierotti, R.A., Rouquerol, J., Siemieniewska, T., 1985. Reporting physisorption data for gas/solid systems with special reference to the determination of surface area and porosity. Pure Appl. Chem. 54, 603–619.

Tanaka, T., Godin, B., Bhavane, R., Nieves-Alicea, R., Gu, J., Liu, X., Chiappini, C., Fakhoury, J.R., Amra, S., Ewing, A., Li, Q., Fidler, I.J., Ferrari, M., 2010a. In vivo evaluation of safety of nanoporous silicon carriers following single and multiple dose intravenous administrations in mice. Int. J. Pharm. 402, 190–197.

Tanaka, T., Mangala, L.S., Vivas-Mejia, P.E., Nieves-Alicea, R., Mann, A.P., Mora, E., Han, H.D., Shahzad, M.M., Liu, X., Bhavane, R., Gu, J., Fakhoury, J.R., Chiappini, C., Lu, C., Matsuo, K., Godin, B., Stone, R.L., Nick, A.M., Lopez-Berestein, G., Sood, A.K., Ferrari, M., 2010b. Sustained small interfering RNA delivery by mesoporous silicon particles. Cancer Res. 70, 3687–3696.

Tonbul, H., Sahin, A., Tavukcuoglu, E., Ultav, G., Akbas, S., Aktas, Y., Esendaglı, G., Capan, Y., 2021. Folic acid decoration of mesoporous silica nanoparticles to increase cellular uptake and cytotoxic activity of doxorubicin in human breast cancer cells. J. Drug Delivery Sci. Technol. 63, 102535.

Tzur-Balter, A., Shatsberg, Z., Beckerman, M., Segal, E., Artzi, N., 2015. Mechanism of erosion of nanostructured porous silicon drug carriers in neoplastic tissues. Nat. Commun. 6, 6208.

Waring, M.J., Arrowsmith, J., Leach, A.R., Leeson, P.D., Mandrell, S., Owen, R.M., Pairaudeau, G., Pennie, W.D., Pickett, S.D., Wang, J., Wallace, O., Weir, A., 2015. An analysis of the attrition of drug candidates from four major pharmaceutical companies. Nat. Rev. Drug Discov. 14, 475–486.

Williams, H.D., Trevaskis, N.L., Charman, S.A., Shanker, R.M., Charman, W.N., Pouton, C.W., Porter, C.J., 2013. Strategies to address low drug solubility in discovery and development. Pharmacol. Rev. 65, 315–499.

Xia, W., Low, P.S., 2010. Folate-targeted therapies for cancer. J. Med. Chem. 53, 6811–6824.

Yan, F., Liang, H., Song, J., Cui, J., Liu, Q., Liu, S., Wang, P., Dong, Y., Liu, H., 2017. Palladium-Catalyzed Cyclization-Heck Reaction of Allenamides: An Approach to 3-Methylene-5-phenyl-1,2,3,4-tetrahydropyridine Derivatives. Org. Lett. 19, 86–89.

Yu, T., Greish, K., McGill, L.D., Ray, A., Ghandehari, H., 2012. Influence of geometry, porosity, and surface characteristics of silica nanoparticles on acute toxicity: their vasculature effect and tolerance threshold. ACS Nano 6, 2289–2301.